Signatures beyond the rotating-wave approximation in retrieving the photoionization time delay from an ω-2ω interferometric method

Mingqing Liu, Xin-Qiang Wang, Lijuan Jia, Pei-Guang Yan, and Wei-Chao Jiang [*]
Institute of Quantum Precision Measurement, College of Physics and Optoelectronic Engineering,
Shenzhen University, Shenzhen 518060, China

We propose a protocol to retrieve the photoionization time delay that employs a pair of oppositely circularly polarized attosecond extreme ultraviolet pulses with frequencies ω and 2ω. By numerically solving the three-dimensional time-dependent Schrödinger equation, we observe an oscillation in the energy-resolved photoionization time delay encoded in the relative optical phase between ω and 2ω pulses when the emission asymmetry of the photoelectron is maximal. Our results show that this oscillation arises from the interference between two one-photon ionization pathways from the ground state due to the broad bandwidth effect of an ultrashort pulse: the absorption of one left-handed circularly polarized photon and the emission of one right-handed circularly polarized photon. The latter is regarded as a consequence of the breakdown of the rotating-wave approximation (RWA). We compare the perturbation theory with and without RWA and demonstrate that photon emission plays a crucial role in retrieving photoionization time delay. Our study enriches the underlying physics of attosecond spectroscopy and provides a framework for accurately measuring photoionization time delays in atoms and molecules.

I. INTRODUCTION

By probing the attosecond photoionization time delays [1–5], which provide precise timing of electronic motion in atoms and molecules [6–8], scientists can observe the electronic evolution in real time [9,10]. The complex photoionization amplitudes describing the transitions between the ground state and the continuum state can fully describe the photoionization process in quantum mechanics. Conventional pump-probe schemes, such as attosecond streaking [11–16] and RABBIT (reconstruction of attosecond beating by interference of two-photon transitions) [17–21], have been proposed to measure the photoemission delay, which can be expressed as the energy derivative of the transition phases of photoionization amplitude [22–24]. Recently, a circular holographic ionization-phase meter [25], which uses pump bicircular attosecond pulse train (APT) in combination with a co- or counter-rotating probe infrared (IR) pulse, and the quantum beat method [26] can provide direct access to complex structures in the energy-resolved phase of ionization amplitudes.

In addition to the above-mentioned schemes involving an IR dressing pulse, an interferometric method without a dressing field, using two phase-locked linearly polarized extreme ultraviolet (XUV) pulses of frequency ω and 2ω, from a free-electron laser, is proposed to precisely determine the absolute phase relationship of a fundamental wavelength and its second harmonic [27] and to measure the angle-resolved photoionization phase [28]. By adjusting the relative optical phase between two pulses, one can achieve the resonant control of photoelectron directionality [29], and even get access to the phase differences of two-photon ionization (TPI) paths involving energetically distant intermediate states [30]. It is well known that the asymmetry in angular distribution of photoelectron is very sensitive to the carrier-envelope phase (CEP) of the few-cycle circularly polarized pulse [31,32], which can be attributed to the interference between one- and two-photon ionization pathways [33,34]. Therefore, the phase difference between one- and two-photon ionization amplitudes can be easily retrieved from the photoemission asymmetry by changing the relative CEP of circularly polarized pulses.

Most theoretical frameworks that describe the components of final states in one- or two-photon ionization employ the rotating-wave approximation (RWA), which takes into account only the corotating field with the system and neglects the counter-rotating part [35,36]. This approximation is often used in the determination of the orbital angular momentum and magnetic quantum number of the partial wave of the scattering states [25,26,29]. For multiphoton ionization processes with the attosecond pulse in the XUV regime and experimentally accessible intensities below 10^{14} W/cm^2, the RWA is valid, i.e., it is legitimate to neglect photon emission processes in the perturbation theory (PT) analysis [37,38] for the circularly polarized XUV pulses. However, in the RABBIT for retrieving the complete phase profiles of attosecond wave packets, the role of IR photon emission cannot be ignored. It is because two-photon pathways (absorption and stimulated emission of an IR photon) can interfere with each other across the whole spectral width of the ultrashort APT. Another recent example is the attosecond transient absorption spectroscopy [39], in which the breakdown of RWA has been clearly seen

─────────
[*]jiang.wei.chao@szu.edu.cn

for a few-cycle XUV pump and near-infrared pulse probe scheme in experiment.

In this work we present an interferometric method, using the right-handed circularly polarized (RCP) pulse with frequency ω and time-delayed left-handed circularly polarized (LCP) pulse with frequency 2ω, to retrieve the energy-resolved photoionization time delay. By varying the relative phase between the two pulses while keeping the pulse delay fixed, the time delay can be extracted from the photoelectron emission asymmetry. We observe an oscillation in the extracted time delay in the numerical solutions of the time-dependent Schrödinger equation (TDSE). The good agreement between TDSE and PT without RWA supports the conclusion that the oscillation arises due to the interference between two one-photon ionization pathways, i.e., the absorption of LCP photon and the emission of RCP photon. The latter clearly demonstrates the breakdown of the RWA. Furthermore, the pulse-delay and pulse-duration dependence of this oscillation are also investigated in this work. Atomic units are used unless explicitly stated.

II. THEORETICAL FRAMEWORK

A. TDSE calculation

The differential ionization probability of atomic hydrogen is obtained by three-dimensional TDSE in the velocity gauge. Here, the split-Lanczos propagator is used to propagate the wave function in time [40–42], which greatly improves the efficiency of the traditional Lanczos propagator by splitting out the centrifugal potential from the Hamiltonian. In our calculations, the wave function is expanded in a product basis with spherical harmonics for the angular part and a finite-element discrete variable representation (FE-DVR) [43–46] for the radial part. To avoid the use of a very large radial box, the wave-splitting technique [47] is adopted. The maximal angular momentum of $\ell_{max} = 12$, the inner radial box size $R_c = 480$ a.u. with maximal box size $R_{max} = 800$ a.u., and the time step of $\Delta t = 0.01$ a.u. are sufficient to ensure the convergence. The vector potential of a pair of oppositely circularly polarized attosecond pulses having the different carrier frequencies, with the second pulse delayed in time by τ,

$$\mathbf{A}(t) = \mathbf{A}_1(t) + \mathbf{A}_2(t - \tau) \equiv f_1(t)\text{Re}[\mathbf{e}_1 e^{-i(\omega_1 t + \phi_1)}]$$
$$+ f_2(t - \tau)\text{Re}\{\mathbf{e}_2 e^{-i[\omega_2(t-\tau) + \phi_2]}\}, \quad (1)$$

as shown in Fig. 1(a). For the jth pulse ($j = 1, 2$), the polarization vector is $\mathbf{e}_j = (\mathbf{e}_x + i\eta_j\mathbf{e}_y)/\sqrt{1 + \eta_j^2}$, where η_j is the ellipticity; here $\eta_j = (-1)^{j+1}$. In our simulation, the laser pulse propagates along the positive z axis and is polarized in the x-y plane. Each pulse has a temporal envelope $f_j(t) = \sqrt{I_j}/\omega_j \cos^2(\frac{\pi t}{T_j})$, where $-T_j/2 \leqslant t \leqslant T_j/2$ with $T_j = n_p\frac{2\pi}{\omega_j}$; n_p is the number of optical cycles. The peak intensity $I_1 = 10I_2 = 1 \times 10^{14}$ W/cm^2 and the frequency $\omega_2 = 2\omega_1 \equiv 2\omega = 20$ eV. ϕ_1 and ϕ_2 denote the respective CEP of two oppositely circularly polarized pulses and $\phi = \phi_2 - \phi_1$ is the relative optical phase.

According to the wave-splitting technology, at the end time t_f of the propagation, we obtain the final ionization amplitude $f(\mathbf{k}, t_f)$ by adding all the amplitudes at time t_f. In
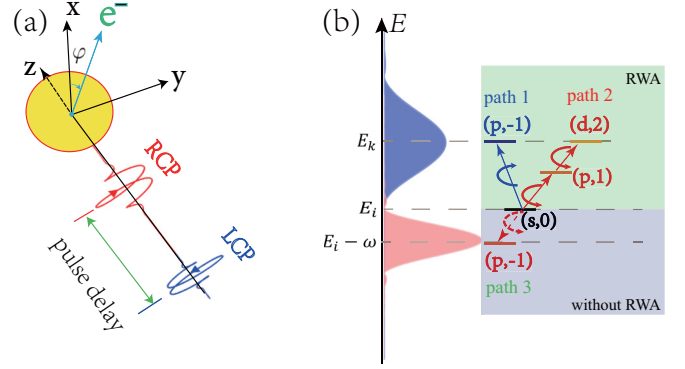

FIG. 1. (a) Geometry of the angularly resolved detection in a pair of time-delayed, oppositely circularly polarized, attosecond laser pulses. Electron is emitted into the polarization plane (x-y) with azimuthal angle φ. The first pulse is right-handed circularly polarized (RCP), while the time-delayed pulse is left-handed circularly polarized (LCP). (b) In the RWA, according to dipole selection rule, the ground state of H atom $(s, 0)$ with the bound energy $E_i = -13.6$ eV absorbs two RCP photons to reach final scattering state $(d, 2)$ (path 2, red solid arrows), which can interfere with $(p, -1)$ state with the same final energy $E_k = 2\omega - I_p$ by absorbing one LCP photon (path 1, blue arrow). The numbers in parentheses denote the angular momentum and magnetic quantum number, respectively. However, without RWA, the scattering state $(p, -1)$ can also be achieved by emitting one RCP photon from the ground state (path 3, red dashed arrow). The two pathways (path 1 and path 3) to create the state $(p, -1)$ interfere with each other due to the large spectral width of the ultrashort attosecond XUV pulse. The blue and red areas denote the frequency spectral range of LCP and RCP pulses, respectively.

the polarization plane, the differential ionization probability $P(E, \theta = \frac{\pi}{2}, \varphi) = k|f(k, \theta = \frac{\pi}{2}, \varphi, t_f)|^2$. The photoelectron asymmetry in the angular distribution is defined as

$$f_a(E) = \frac{P(E, \varphi)_{0 \leqslant \varphi \leqslant 180°} - P(E, \varphi)_{180° \leqslant \varphi \leqslant 360°}}{P(E, \varphi)_{0 \leqslant \varphi \leqslant 180°} + P(E, \varphi)_{180° \leqslant \varphi \leqslant 360°}}, \quad (2)$$

which gives the difference of electron yield emitted into opposite sides of the plane parallel to the light polarization.

B. Photoelectron emission asymmetry calculated by PT

The well-known electric dipole selection rules state that the absorption of one photon leads to the electron angular momentum changing by one unit, $\Delta\ell = \pm 1$ [48,49]. For the magnetic quantum number, in the RWA, it increases by one unit ($\Delta m = +1$) for absorption of one RCP photon while decreasing by one unit ($\Delta m = -1$) for absorption of one LCP photon. One-photon ionization of the hydrogen atom from its ground state $|\ell = 0, m = 0\rangle$ [denoted by $(s, 0)$] by absorbing one LCP photon creates a continuum wave at the energy $E_k = 2\omega - I_p$ with angular momentum quantum numbers $\ell = 1$, $m = -1 \sim Y_{1-1}(\theta, \varphi)$. $Y_{\ell m}(\theta, \varphi)$ is the spherical harmonics function. The same energy can be reached via a two-photon absorption from the RCP pulse; the angular dependence of the continuum wave populated by the two-photon path is $Y_{22}(\theta, \varphi)$, as shown in Fig. 1(b) (solid lines).

However, without the RWA, the transition from the ground state to the partial wave ($\ell = 1, m = -1$) also occurs by emitting one RCP photon, as shown by the dashed arrow in Fig. 1(b). For the ultrashort attosecond XUV pulses employed here with larger spectral width, the one-photon pathway with releasing one RCP photon of the energy ω can interfere with the one-photon pathway with absorbing one LCP photon of the energy 2ω. The spectral width $\Delta\omega = 1.44\omega/n_p$ for RCP and LCP pulses for $n_p = 2$ are 14.4 and 7.2 eV, respectively [50,51]. As shown in Fig. 1(b), the long tail in a broad bandwidth with a central energy $E_i - \omega$ of RCP XUV pulse overlaps with the frequency spectra of LCP XUV pulse with a central energy E_k. As can be seen below, even though the transition amplitudes of the final state $(p, -1)$ contributed from RCP pulse (path 3) is less than that from LCP (path 1) by about two orders of magnitude, this tiny overlap has a significant influence on the energy-dependent amplitude phases.

The one-photon transition amplitude calculated by the time-dependent PT in velocity gauge is given by

$$\mathcal{A}_1(\mathbf{k}) = -\int_{t_i}^{t_f} \langle\Psi_{\mathbf{k}}|\mathbf{A}(t')\cdot\nabla|\Psi_i\rangle e^{i(E-E_i)t'}dt', \quad (3)$$

where $|\Psi_{\mathbf{k}}\rangle$ is the final scattering state with asymptotic momentum $\mathbf{k}$, $E = k^2/2$, and $|\Psi_i\rangle$ is the initial ground state with energy $E_i = -13.6$ eV. $t_i = -T_1/2$, and $t_f = \tau + T_2/2$. The contribution to the one-photon amplitude from the RCP pulse is

$$\mathcal{A}_1^R(\mathbf{k}) = -\int_{t_i}^{t_f} \langle\Psi_{\mathbf{k}}|\mathbf{A}_1(t')\cdot\nabla|\Psi_i\rangle e^{i(E-E_i)t'}dt'$$
$$= [-g_1^-(\omega)Y_{11} + g_1^+(\omega)Y_{1-1}]. \quad (4)$$

Here,

$$g_1^{\pm}(\omega) = -\frac{\sqrt{2I_1}}{2\sqrt{3}}(E-E_i)\langle\psi_k|r|\psi_i\rangle$$
$$\times \frac{1}{\omega}\int_{-T_1/2}^{T_1/2}\cos^2\left(\frac{\pi t}{T_1}\right)\exp[i(E-E_i\pm\omega)t]dt, \quad (5)$$

where $|\psi_i\rangle$ and $|\psi_k\rangle$ are the radial wave function of initial and final states, respectively [34]. The superscript symbols "+" and "−" in $g_1(\omega)$ clearly indicate the emission and absorption of the photon, respectively. Likewise, the contribution to the one-photon amplitude from the LCP pulse can be expressed as

$$\mathcal{A}_1^L(\mathbf{k}) = -\int_{t_i}^{t_f} \langle\Psi_{\mathbf{k}}|\mathbf{A}_2(t')\cdot\nabla|\Psi_i\rangle e^{i(E-E_i)t'}dt'$$
$$= [-g_2^+(\omega)Y_{11} + g_2^-(\omega)Y_{1-1}], \quad (6)$$

where

$$g_2^{\pm}(\omega) = -\frac{\sqrt{2I_2}}{2\sqrt{3}}(E-E_i)\langle\psi_k|r|\psi_i\rangle e^{i(E-E_i)\tau}e^{\pm i\phi}$$
$$\times \frac{1}{2\omega}\int_{-T_2/2}^{T_2/2}\cos^2\left(\frac{\pi t}{T_2}\right)\exp[i(E-E_i\pm 2\omega)t]dt. \quad (7)$$

Comparing Eq. (5) with Eq. (7), the main difference between $g_2(\omega)$ and $g_1(\omega)$ is the introduction of phase

factor $(E - E_i)\tau \pm \phi$, which includes the information of pulse delay τ and relative CEP ϕ.

For the two-photon absorption process, the corresponding transition amplitude is given by

$$\mathcal{A}_2(\mathbf{k}) = \sum_{q\neq i}\int_{t_i}^{t_f}dt'\langle\Psi_{\mathbf{k}}|\mathbf{A}(t')\cdot\nabla|\Psi_q\rangle e^{i(E-E_q)t'}$$
$$\times \int_{t_i}^{t'}dt''\langle\Psi_q|\mathbf{A}(t'')\cdot\nabla|\Psi_i\rangle e^{i(E_q-E_i)t''}, \quad (8)$$

where $|\Psi_q\rangle$ with energy E_q is the intermediate state. In our PT calculations, the wave functions of initial state and each intermediate eigenstate are obtained by the diagonalization of a free-field Hamiltonian, which is discretized using the FE-DVR representation method. In the calculation of two-photon amplitude, the radial box size of $R_{\max} = 50$ a.u., the first 100 intermediate eigenstates are chosen within the total 300 intermediate eigenstates, which already ensure the convergence of calculation. The numbers of finite element and basis functions are 50 and 7, respectively. The final scattering states are obtained analytically as shown in Ref. [52].

The angle-dependent ionization probability obtained from PT is

$$P(E, \varphi) = k|\mathcal{A}_1(\mathbf{k}) + \mathcal{A}_2(\mathbf{k})|^2, \quad (9)$$

where $\mathcal{A}_1(\mathbf{k}) \equiv c_{\ell=1}e^{is_{\ell=1}}$ and $\mathcal{A}_2(\mathbf{k}) \equiv c_{\ell=2}e^{is_{\ell=2}}$. Therefore, the transition amplitudes with $\ell = 1$ and $\ell = 2$ are written as

$$c_{\ell=1}e^{is_{\ell=1}} = c_{p,1}e^{is_{p,1}}Y_{11} + c_{p,-1}e^{is_{p,-1}}Y_{1-1}e^{-i\phi}, \quad (10)$$

$$c_{\ell=2}e^{is_{\ell=2}} = c_{d,2}e^{is_{d,2}}Y_{22}, \quad (11)$$

where $c_{p,1}$, $c_{p,-1}$, and $c_{d,2}$ are the real-value partial wave amplitudes; $s_{p,1}$, $s_{p,-1}$, and $s_{d,2}$ are the corresponding arguments. Note that in two-photon ionization only the partial wave $(d, 2)$ is considered due to the trivial contribution from the other partial waves, such as $(s, 0)$ and $(d, 0)$. Therefore, the energy-resolved asymmetry $f_a(E)$ defined by Eq. (2) can be rewritten as

$$f_a(E) = \frac{2\sqrt{5}/\pi}{c_{p,1}^2 + c_{p,-1}^2 + 5c_{d,2}^2/4}\rho(\phi), \quad (12)$$

where the ϕ-dependent term

$$\rho(\phi) = c_{p,1}c_{d,2}\sin(s_{d,2} - s_{p,1})$$
$$- \tfrac{1}{3}c_{p,-1}c_{d,2}\sin[\phi + (s_{d,2} - s_{p,-1})]. \quad (13)$$

C. Retrieving time delay in PT with and without RWA

In the RWA, the photon emission process is ignored; then

$$c_{p,1}\exp\left(is_{p,1}^{\mathrm{RWA}}\right) = -g_1^-(\omega), \quad (14)$$

$$c_{p,-1}\exp\left(is_{p,-1}^{\mathrm{RWA}}\right)e^{-i\phi} = g_2^-(\omega). \quad (15)$$

In the perturbative regime, the one-photon ionization amplitude phase for single circularly polarized pulse is equal to $3\pi/2 + \sigma_1$ [34], where $\sigma_1 = \arg\Gamma(2 - i/k)$ is the r-independent Coulomb phase shift [53]. From the lowest-order perturbation theory respective, the phases $s_{p,1}$ and $s_{p,-1}$ originate from the RCP and LCP pulse, respectively, which can be

expressed as

$$s_{p,1}^{\mathrm{RWA}} = \frac{3\pi}{2} + \sigma_1, \tag{16}$$

$$s_{p,-1}^{\mathrm{RWA}} = \frac{3\pi}{2} + \sigma_1 + (E - E_i)\tau. \tag{17}$$

Thus the ϕ-dependent term in Eq. (13) only exists in the factor $\sin[\phi + (s_{d,2} - s_{p,-1})]$, so the asymmetry reaches its maximal value when $\phi = \phi_{\mathrm{m}}$, where

$$\phi_{\mathrm{m}} = (s_{p,-1} - s_{d,2}) - \frac{\pi}{2} + n2\pi. \tag{18}$$

n is an integer number. Note that Eq. (18) demonstrates the fundamental principle about retrieving the photoionization time delay, i.e., the transition phase difference can be directly extracted from the ω-2ω relative phase corresponding to the maximal photoelectron emission asymmetry.

However, for the situation where the breakdown of RWA occurs, the amplitude of partial wave $(p, -1)$ with taking the photon emission into account is

$$c_{p,-1}e^{is_{p,-1}}e^{-i\phi} = g_1^+(\omega) + g_2^-(\omega)$$
$$= M_R e^{i\Phi_R} + M_L e^{i\Phi_L}e^{-i\phi}, \tag{19}$$

where M_L, Φ_L and M_R, Φ_R are the transition amplitudes and phases from the ground state to the specific partial wave $(p, -1)$ by absorbing one LCP photon and releasing one RCP photon [dashed line in Fig. 1(b)], respectively. By Eqs. (5) and (7), we obtain $\Phi_L = \frac{3\pi}{2} + \sigma_1 + (E - E_i)\tau$ and $\Phi_R = \frac{3\pi}{2} + \sigma_1$. Hence

$$c_{p,-1}e^{is_{p,-1}}e^{-i\phi} = M_L e^{i(\frac{3\pi}{2}+\sigma_1)}e^{-i\phi}[e^{i(E-E_i)\tau} + \chi \, e^{i\phi}]$$
$$= DM_L e^{i(\frac{3\pi}{2}+\sigma_1)}e^{i\Theta}e^{-i\phi}, \tag{20}$$

where $\chi = M_R/M_L$; D and Θ are the module and argument of $e^{i(E-E_i)\tau} + \chi e^{i\phi}$, respectively. Thus the module and phase of amplitude of partial wave $(p, -1)$ without RWA can be rewritten as

$$c_{p,-1} = M_L\sqrt{1 + \chi^2 + 2\chi \, \cos(\beta - \phi)}, \tag{21}$$

$$s_{p,-1} = \frac{3\pi}{2} + \sigma_1 + \Theta, \tag{22}$$

where $\tan\Theta = (\sin\beta + \chi \, \sin\phi)/(\cos\beta + \chi \, \cos\phi)$ and $\beta = (E - E_i)\tau$.

The Wigner time delay of one-photon ionization, τ_W, corresponds to the energy derivative of the argument of the amplitude, $\tau_W = ds_{p,-1}/dE$. To better compare with the RWA results [Eq. (17)], we introduce $\tilde{s}_{p,-1} \equiv s_{p,-1} - (E - E_i)\tau$; hence

$$\frac{d\tilde{s}_{p,-1}}{dE} = \frac{d\sigma_1}{dE} + \frac{d\Theta}{dE} - \tau, \tag{23}$$

where the τ-dependent term

$$\frac{d\Theta}{dE} - \tau \approx -\chi\tau \, \cos(\beta - \phi) - \frac{d\chi}{dE}\sin(\beta - \phi). \tag{24}$$

In the deduction of Eq. (24), χ^2 term is ignored and $1 + 2\chi \, \cos(\beta - \phi) \approx 1$ is employed due to the fact that the order of magnitudes of χ is about 10^{-2}, as is shown below. Note that Eq. (24) denotes the contribution of
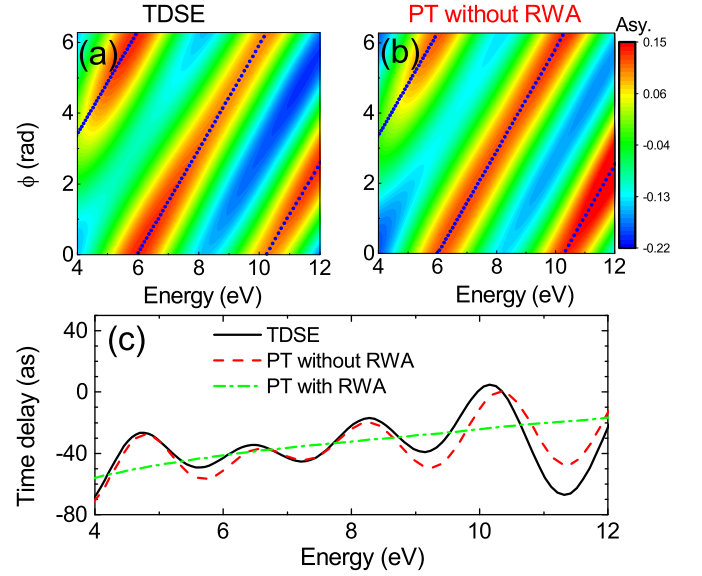

FIG. 2. Photoelectron angular asymmetry $f_a(E)$ defined by Eq. (2) as functions of energy E and relative optical phase ϕ calculated by (a) TDSE and (b) complete PT (without RWA). The pulse time delay $\tau = 1$ fs and $n_p = 2$. The blue dots in (a) and (b) denote the specific relative phase ϕ_{m}, where the asymmetry reaches its maximum for each electron energy. (c) Extracted time delay $d\tilde{\phi}_{\mathrm{m}}/dE$ as a function of energy E obtained from TDSE and two types of PT calculations, where $\tilde{\phi}_{\mathrm{m}} = \phi_{\mathrm{m}} - (E - E_i)\tau$. The PT calculation with RWA denotes that the amplitudes of partial wave $(p, -1)$ are obtained by ignoring the photon emission process.

the RCP pulse to the amplitude phase of partial wave $(p, -1)$. Therefore, the photoionization time delay can be rewritten as $d\tilde{\phi}_{\mathrm{m}}/dE = d\phi_{\mathrm{m}}/dE - \tau = d[s_{p,-1} - s_{d,2} - (E - E_i)\tau]/dE$, where $\tilde{\phi}_{\mathrm{m}} = \phi_{\mathrm{m}} - (E - E_i)\tau$.

III. RESULTS AND DISCUSSION

Figures 2(a) and 2(b) represent the energy-dependent asymmetries in the angular distribution of photoelectrons as a function of the relative optical phase ϕ. Both the three-dimensional TDSE and complete PT (without RWA) calculations exhibit three straight stripes with two intersections at energies $E = 6.0$ and 10.3 eV in the photoelectron emission asymmetry. These stripes indicate that, as the energy increases, the corresponding ϕ_{m} denoting the maximal photoemission asymmetry of each energy, shown by the blue dots, almost linearly increases. According to Eq. (18), the photoionization time delay between one- and two-photon ionizations, which can be expressed as the derivative of $\tilde{\phi}_{\mathrm{m}}$ with respect to energy E, is the slope of stripes minus the pulse delay τ.

However, we find a counterintuitive phenomenon where the time delay extracted from the maximal asymmetry shows an obvious oscillation, as shown in Fig. 2(c). This oscillation implies that the increase of ϕ_{m} is not strictly linear with the increasing energy. In Fig. 2(c), we display two types of PT calculations, i.e., without and with RWA. The PT calculation without RWA quantitatively agrees with TDSE results, while for the PT calculation with RWA, the time delay $d\tilde{\phi}_{\mathrm{m}}/dE$ increases smoothly as energy increases.
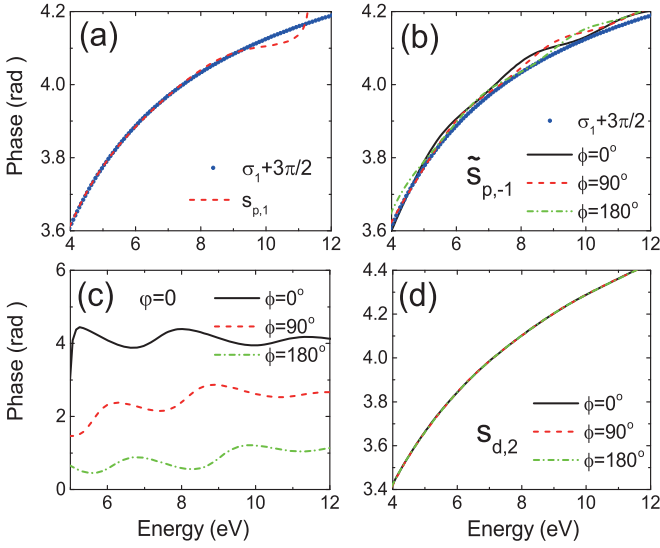
FIG. 3. Energy-dependent one-photon amplitude phases (a) $s_{p,1}$, (b) $\tilde{s}_{p,-1} = s_{p,-1} - (E - E_i)\tau$, (c) $\tilde{s}_{\ell=1} = s_{\ell=1} - (E - E_i)\tau$ for $\varphi = 0$, and (d) two-photon amplitude phase $s_{d,2}$ when the relative phase ϕ varies, which are calculated by PT without RWA.

For the one-photon amplitude in two kinds of PT calculations, we chose the partial waves of final scattering states with $\ell = 1$ and $m = \pm 1$ and, for the two-photon amplitude, we chose the single partial wave with $\ell = 2$ and $m = 2$. In the RWA, from Eqs. (17) and (18), $d\tilde{\phi}_m/dE = d\sigma_1/dE - ds_{d,2}/dE$. In Figs. 3(a) and 3(d), we show the energy dependence of the amplitude phases $s_{p,1}$ and $s_{d,2}$, respectively. It can be seen that $s_{p,1}$ is in accordance with $3\pi/2 + \sigma_1$ and $s_{d,2}$ increases smoothly and is independent of the relative phase ϕ. Note that the deviation between $s_{p,1}$ and $3\pi/2 + \sigma_1$ for $E > 10$ eV is due to the fact that this energy range is far away from the first-order above-threshold ionization (ATI) peak ($E = 6.4$ eV), resulting in the lowest-order PT not being able to describe well the one-photon ionization.

It is natural to believe that the oscillation in the time delay comes from the transition phase $s_{p,-1}$. To better understand the underlying picture of this oscillation, we plot the one-photon amplitude phases $s_{p,-1}$ and $s_{\ell=1}$ calculated by the complete PT in Figs. 3(b) and 3(c), respectively. In the RWA, $\tilde{s}_{p,-1} = 3\pi/2 + \sigma_1$ increases smoothly with the increasing energy. However, in our PT calculation without RWA, even though $\tilde{s}_{p,-1}$ is almost equal to $3\pi/2 + \sigma_1$, it displays a clear oscillation and strongly depends on the relative phase ϕ. In Fig. 3(c), for the azimuthal angle $\varphi = 0$ ($Y_{11} = -Y_{1-1}$), the one-photon ionization phase $\tilde{s}_{\ell=1}$ of each energy gradually decreases when the relative phase ϕ changes from 0 to π due to the factor $\exp(-i\phi)$ in Eq. (10). Furthermore, the out-of-phase oscillations of phase $\tilde{s}_{\ell=1}$ between $\phi = 0$ and π can be also clearly observed. This out-of-phase oscillation can be explained well by the relation deduced from Eq. (24), which states that $d\tilde{s}_{p,-1}/dE|_{\phi=0} = -d\tilde{s}_{p,-1}/dE|_{\phi=\pi}$. These aforementioned observations suggest that the oscillation in time delay is primarily caused by the fluctuation in the one-photon ionization phase $\tilde{s}_{p,-1}$.

According to our analytical formula Eq. (19), the amplitude phase $s_{p,-1}$ is not solely determined by the LCP pulse,
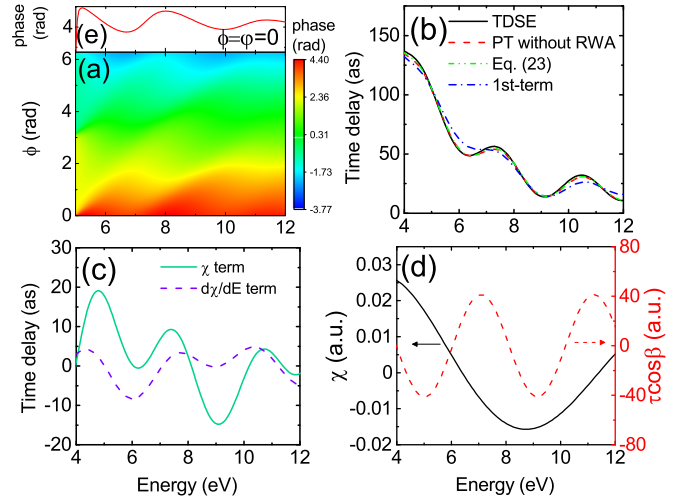

FIG. 4. (a) One-photon amplitude phase $\tilde{s}_{\ell=1}$ when $\varphi = 0$ as functions of relative phase ϕ and energy E with $s_{p,-1}$ is obtained by Eq. (22); the red line in (e) denotes the $\tilde{s}_{\ell=1}$ of $\phi = 0$, which is extracted from (a) for comparing with Fig. 3(c). (b) Comparison of time delay $d\tilde{s}_{p,-1}/dE$ obtained from TDSE, PT without RWA, and the analytical formula [Eq. (23)], where the "1st-term" line denotes that the contribution of the first term in Eq. (24). (c) The respective contribution of the first term (solid line) and second term (dashed line) in Eq. (24) when $\phi = 0$. (d) Energy dependent amplitude ratio χ (black solid line) and only τ-dependent term $\tau\cos\beta$ (red dashed line).

but is also influenced by the contribution from the RCP pulse, which falls beyond the RWA. By comparing TDSE and PT calculations without RWA, we have confirmed that $c_{p,1}$, $s_{p,1}$, $c_{d,2}$, and $s_{d,2}$ remain independent of ϕ, whereas $c_{p,-1}$ and $s_{p,-1}$ are affected by ϕ, as evidenced by Eqs. (21) and (22). By using Eqs. (21) and (22) to calculate the transition amplitudes $c_{p,-1}$ and phases $s_{p,-1}$ in Eq. (10), we obtain the one-photon amplitude phase $s_{\ell=1}$ that agrees excellently with PT calculations without RWA, as shown by Figs. 4(a) and 4(e). Note that this agreement holds for other relative phases (not presented here). In Fig. 4(b), the sensitivity of $s_{p,-1}$ to energy is evident from the derivative of $\tilde{s}_{p,-1}$ with respect to energy E. The amplitude phases $s_{p,-1}$ of TDSE can be obtained by projecting calculations that only include the final partial wave $|\ell = 1, m = -1\rangle$. For PT results, $s_{p,-1}$ is calculated by first-order PT in the velocity gauge with the total vector potential $\mathbf{A}(t)$ [Eq. (1)]. The excellent consistency of $d\tilde{s}_{p,-1}/dE$ between TDSE and the analytical formula indicates that the oscillation of one-photon ionization time delay primarily arises from the interference between ionization amplitudes resulting from the emission of RCP photon and the absorption of LCP photon, respectively.

The dominant role of the first term in Eq. (24) is shown by the line denoted as "1st-term" in Fig. 4(b). As seen in Fig. 4(c), for $\phi = 0$, the χ term of $d\Theta/dE - \tau$ can reproduce well the oscillation of $d\tilde{s}_{p,-1}/dE$. This is due to the fact that the oscillation of $d\chi/dE$ term is almost in phase with that of χ term and the value of $d\chi/dE$ term oscillates around zero as the energy varies. The χ term comprises the amplitude ratio χ and τ-dependent term $\cos[(E - E_i)\tau]$, which are separated and displayed in Fig. 4(d). It is clear that, in contrast to the
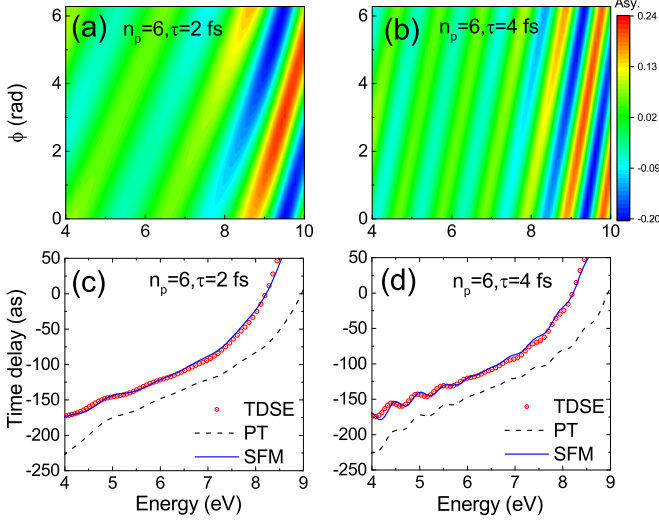
FIG. 5. Energy-dependent asymmetry $f_a(E)$ as a function of relative optical phase ϕ calculated by TDSE for different pulse delays (a) $\tau = 2$ fs and (b) $\tau = 4$ fs with a longer pulse duration $n_p = 6$. Extracted time delay $d\tilde{\phi}_m/dE$ as a function of energy E from TDSE and complete PT calculations for (c) $\tau = 2$ fs and (d) $\tau = 4$ fs with $n_p = 6$. Also shown are the results of the strong-field model (SFM) in which the depletion of ground state is considered. See text for the details.

periodic oscillation of $\cos[(E - E_i)\tau]$, the ratio χ oscillates much slower with photoelectron energy. Therefore, the oscillation period of $d\tilde{\phi}_m/dE$ largely depends on the τ-dependent term $\cos[(E - E_i)\tau]$ and it can be predicated that this oscillation period decreases as the pulse delay τ increases.

For the multicycle pulse (e.g., $n_p = 6$), this oscillation can also be observed provided that the pulse time delay τ is large enough. It can be seen from Figs. 5(a) and 5(b) that the number of the straight stripes increases significantly with the increasing τ and the larger asymmetries are mostly concentrated at higher energies. The time delay extracted from these separated stripes shows clear oscillation as the electron energy varies for two larger pulse delays (2 fs and 4 fs) as shown in Figs. 5(c) and 5(d), respectively. Similarly, PT without RWA still can reproduce well the peaks and rising tendency of oscillation as shown by TDSE. Both TDSE and PT without RWA calculations demonstrate that the photoionization time delay of the multicycle pulse increases much faster than the few-cycle pulse and the oscillation period becomes much smaller with increasing τ for the same pulse duration, as predicated by Eq. (24). However, the time delay obtained by PT differs quantitatively from that calculated by TDSE, which can be attributed to the depletion of the ground state. In our TDSE calculation, the population of the ground state drops by about 70% at the end of the pulse. To overcome this, we use the nonperturbative strong-field model (SFM) proposed in our previous works [34,41,54,55], in which the wave function of the ground state $|\Psi_i(t')\rangle$ is replaced by $h(t')|\Psi_i(t')\rangle$ in Eqs. (3) and (8), where $h(t')$ is the modulus of the amplitude of the ground state at time t'. The SFM calculation with considering the depletion of the ground state can quantitatively reproduce the corresponding TDSE results, as shown in Figs. 5(c) and 5(d).
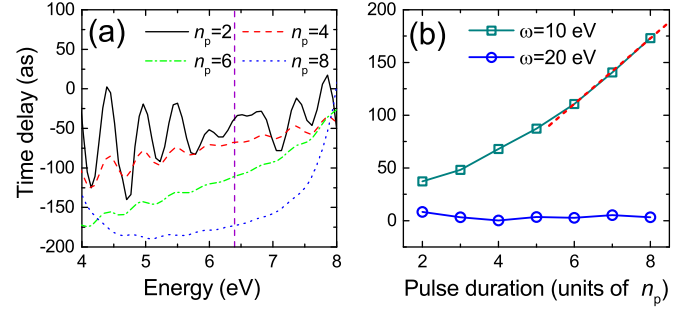

FIG. 6. (a) Energy-dependent time delay $d\tilde{\phi}_m/dE$ extracted from the angular asymmetry calculated by TDSE for different pulse durations $n_p = 2, 4, 6, 8$ with $\tau = 4$ fs. The vertical line denotes the final-state energy of photoelectron in TPI, which is $2\omega - I_p = 6.4$ eV. (b) Time delay extracted from (a) for the TPI signal as a function of the XUV pulse duration when photon energies $\omega = 10$ eV ($E = 6.4$ eV) and $\omega = 20$ eV ($E = 26.4$ eV), respectively.

We also investigate the XUV pulse duration dependence of time delays retrieved from maximal asymmetry, as shown in Fig. 6(a). The obtained results show that the oscillation weakens as the XUV pulse duration increases and even becomes smooth until the spectral widths of two XUV pulse no longer overlap with each other due to the spectral width $\Delta\omega = 1.44\omega/n_p$ for the cosine-squared pulse envelope. We find that the time delay increases significantly for longer pulse durations. Note that in Fig. 5, the ionization delay of $n_p = 6$ just shifts up about 25 attoseconds due to depletion as compared to that of $n_p = 2$. However, in Fig. 6(a), the ionization delay of $n_p = 6$ decreases about 73 attoseconds in the combined influence from depletion and resonance contribution from $2p$. It can be known that the influence of resonance on ionization delay dominates as compared to the influence of depletion, which may be due to the depletion influence being the time-averaged effect according to Eqs. (3) and (8). In Fig. 6(b), we plot the time delay extracted from Fig. 6(a) at energy $E = 6.4$ eV for TPI (here we change the sign of time delay to better observe time delay of TPI). For photon energy $\omega = 10$ eV the time delay has a significant change that scales nearly linearly with the XUV pulse duration once the pulse is long enough ($T_1 > 2.48$ fs, as shown by red dashed line). The photon energy of $\omega = 10$ eV is close to the energy difference between the ground state and the first excited state $2p$ of the H atom, which is 10.2 eV. However, for the photon energy $\omega = 20$ eV, in which the resonant effect is ruled out, the retrieved time delays are nearly independent of the XUV pulse duration. The XUV pulse duration dependence of time delays in TPI was also studied previously in Ref. [56], in which the time delays in a resonant and nonresonant TPI of the helium atom are simulated numerically by using the attosecond streaking technique. Therefore, our methods can reproduce well the XUV pulse duration dependence of time delays in the resonant and nonresonant TPI.

IV. CONCLUSIONS

In summary, we have theoretically investigated the ω-2ω interferometric protocol for retrieving the photoionization time delay, which utilizes a pair of oppositely circularly

polarized attosecond XUV pulses. In this interferometric protocol, the photoionization time delay can be retrieved from the relative optical ω-2ω phase when the photoelectron emission asymmetry reaches its maximum. The oscillatory structure of the retrieved energy-resolved time delay is observed through the numerical solutions of the TDSE. Based on PT calculation with and without RWA, we find that this oscillation can be attributed to the breakdown of the RWA, which manifests as the interference between two one-photon ionization paths named the absorption of LCP photon and the emission of RCP photon. Furthermore, our analysis also reveals that this oscillation depends strongly on the delay

between the two pulses and the XUV pulse duration. The obtained results provide insights into the retrieval of photoionization time delay in attosecond science when the RWA is invalid.

ACKNOWLEDGMENT

[1] P. Eckle, A. Pfeiffer, C. Cirelli, A. Staudte, R. Dorner, H. Muller, M. Buttiker, and U. Keller, Attosecond ionization and tunneling delay time measurements in helium, Science **322**, 1525 (2008).

[2] M. Schultze, M. Fieß, N. Karpowicz, J. Gagnon, M. Korbman, M. Hofstetter, S. Neppl, A. L. Cavalieri, Y. Komninos, T. Mercouris *et al.*, Delay in photoemission, Science **328**, 1658 (2010).

[3] M. Sabbar, S. Heuser, R. Boge, M. Lucchini, T. Carette, E. Lindroth, L. Gallmann, C. Cirelli, and U. Keller, Resonance Effects in Photoemission Time Delays, Phys. Rev. Lett. **115**, 133001 (2015).

[4] J. Rist, K. Klyssek, N. M. Novikovskiy, M. Kircher, I. Vela-Pérez, D. Trabert, S. Grundmann, D. Tsitsonis, J. Siebert, A. Geyer *et al.*, Measuring the photoelectron emission delay in the molecular frame, Nat. Commun. **12**, 6657 (2021).

[5] J. Fuchs, N. Douguet, S. Donsa, F. Martin, J. Burgdörfer, L. Argenti, L. Cattaneo, and U. Keller, Time delays from one-photon transitions in the continuum, Optica **7**, 154 (2020).

[6] G. Sansone, F. Kelkensberg, J. Pérez-Torres, F. Morales, M. F. Kling, W. Siu, O. Ghafur, P. Johnsson, M. Swoboda, E. Benedetti *et al.*, Electron localization following attosecond molecular photoionization, Nature (London) **465**, 763 (2010).

[7] M. Isinger, R. Squibb, D. Busto, S. Zhong, A. Harth, D. Kroon, S. Nandi, C. Arnold, M. Miranda, J. M. Dahlström *et al.*, Photoionization in the time and frequency domain, Science **358**, 893 (2017).

[8] J. Vos, L. Cattaneo, S. Patchkovskii, T. Zimmermann, C. Cirelli, M. Lucchini, A. Kheifets, A. S. Landsman, and U. Keller, Orientation-dependent stereo wigner time delay and electron localization in a small molecule, Science **360**, 1326 (2018).

[9] R. Pazourek, S. Nagele, and J. Burgdörfer, Attosecond chronoscopy of photoemission, Rev. Mod. Phys. **87**, 765 (2015).

[10] P. K. Maroju, M. D. Fraia, O. Plekan, M. Bonanomi, B. Merzuk, D. Busto, I. Makos, M. Schmoll, R. Shah, P. R. Ribič, L. Giannessi, G. D. Ninno, C. Spezzani, G. Penco, A. Demidovich, M. Danailov, M. Coreno, M. Zangrando, A. Simoncig, M. Manfredda *et al.*, Attosecond coherent control of electronic wave packets in two-colour photoionization using a novel timing tool for seeded free-electron laser, Nat. Photon. **17**, 200 (2023).

[11] M. Drescher, M. Hentschel, R. Kienberger, G. Tempea, C. Spielmann, G. A. Reider, P. B. Corkum, and F. Krausz, X-ray

pulses approaching the attosecond frontier, Science **291**, 1923 (2001).

[12] M. Hentschel, R. Kienberger, C. Spielmann, G. A. Reider, N. Milosevic, T. Brabec, P. Corkum, U. Heinzmann, M. Drescher, and F. Krausz, Attosecond metrology, Nature (London) **414**, 509 (2001).

[13] J. Itatani, F. Quéré, G. L. Yudin, M. Y. Ivanov, F. Krausz, and P. B. Corkum, Attosecond Streak Camera, Phys. Rev. Lett. **88**, 173903 (2002).

[14] R. Kienberger, E. Goulielmakis, M. Uiberacker, A. Baltuska, V. Yakovlev, F. Bammer, A. Scrinzi, T. Westerwalbesloh, U. Kleineberg, U. Heinzmann *et al.*, Atomic transient recorder, Nature (London) **427**, 817 (2004).

[15] P.-L. He, C. Ruiz, and F. He, Carrier-Envelope-Phase Characterization for an Isolated Attosecond Pulse by Angular Streaking, Phys. Rev. Lett. **116**, 203601 (2016).

[16] J. Yan, W. Xie, M. Li, K. Liu, S. Luo, C. Cao, K. Guo, W. Cao, P. Lan, Q. Zhang, Y. Zhou, and P. Lu, Photoelectron ionization time of aligned molecules clocked by attosecond angular streaking, Phys. Rev. A **102**, 013117 (2020).

[17] P.-M. Paul, E. S. Toma, P. Breger, G. Mullot, F. Augé, P. Balcou, H. G. Muller, and P. Agostini, Observation of a train of attosecond pulses from high harmonic generation, Science **292**, 1689 (2001).

[18] H. G. Muller, Reconstruction of attosecond harmonic beating by interference of two-photon transitions, Appl. Phys. B **74**, s17 (2002).

[19] M. Swoboda, T. Fordell, K. Klünder, J. M. Dahlström, M. Miranda, C. Buth, K. J. Schafer, J. Mauritsson, A. L'Huillier, and M. Gisselbrecht, Phase Measurement of Resonant Two-Photon Ionization in Helium, Phys. Rev. Lett. **104**, 103003 (2010).

[20] K. Klünder, J. M. Dahlström, M. Gisselbrecht, T. Fordell, M. Swoboda, D. Guénot, P. Johnsson, J. Caillat, J. Mauritsson, A. Maquet, R. Taïeb, and A. L'Huillier, Probing Single-Photon Ionization on the Attosecond Time Scale, Phys. Rev. Lett. **106**, 143002 (2011).

[21] X. Gong, W. Jiang, J. Tong, J. Qiang, P. Lu, H. Ni, R. Lucchese, K. Ueda, and J. Wu, Asymmetric Attosecond Photoionization in Molecular Shape Resonance, Phys. Rev. X **12**, 011002 (2022).

[22] E. P. Wigner, Lower limit for the energy derivative of the scattering phase shift, Phys. Rev. **98**, 145 (1955).

[23] F. T. Smith, Lifetime matrix in collision theory, Phys. Rev. **118**, 349 (1960).

[24] I. A. Ivanov, Time delay in strong-field photoionization of a hydrogen atom, Phys. Rev. A **83**, 023421 (2011).

[25] S. Donsa, N. Douguet, J. Burgdörfer, I. Březinová, and L. Argenti, Circular Holographic Ionization-Phase Meter, Phys. Rev. Lett. **123**, 133203 (2019).

[26] J. Fuchs, N. Douguet, S. Donsa, F. Martín, J. Burgdörfer, L. Argenti, L. Cattaneo, and U. Keller, Towards the complete phase profiling of attosecond wave packets, Phys. Rev. Res. **3**, 013195 (2021).

[27] M. Di Fraia, O. Plekan, C. Callegari, K. C. Prince, L. Giannessi, E. Allaria, L. Badano, G. De Ninno, M. Trovo, B. Diviacco *et al.*, Complete Characterization of Phase and Amplitude of Bichromatic Extreme Ultraviolet Light, Phys. Rev. Lett. **123**, 213904 (2019).

[28] D. You, K. Ueda, E. V. Gryzlova, A. N. Grum-Grzhimailo, M. M. Popova, E. I. Staroselskaya, O. Tugs, Y. Orimo, T. Sato, K. L. Ishikawa *et al.*, New Method for Measuring Angle-Resolved Phases in Photoemission, Phys. Rev. X **10**, 031070 (2020).

[29] Y. Wang and C. H. Greene, Resonant control of photoelectron directionality by interfering one- and two-photon pathways, Phys. Rev. A **103**, 053118 (2021).

[30] M. Žitnik, A. Mihelič, K. Bučar, Š. Krušič, R. Squibb, R. Feifel, I. Ismail, P. Lablanquie, J. Palaudoux, O. Plekan *et al.*, Interference of two-photon transitions induced by xuv light, Optica **9**, 692 (2022).

[31] D. B. Milošević, G. G. Paulus, and W. Becker, Phase-Dependent Effects of a Few-Cycle Laser Pulse, Phys. Rev. Lett. **89**, 153001 (2002).

[32] S. Fukahori, T. Ando, S. Miura, R. Kanya, K. Yamanouchi, T. Rathje, and G. G. Paulus, Determination of the absolute carrier-envelope phase by angle-resolved photoelectron spectra of Ar by intense circularly polarized few-cycle pulses, Phys. Rev. A **95**, 053410 (2017).

[33] E. A. Pronin, A. F. Starace, M. V. Frolov, and N. L. Manakov, Perturbation theory analysis of attosecond photoionization, Phys. Rev. A **80**, 063403 (2009).

[34] M. Liu, S. U. Khan, X.-Q. Wang, P.-G. Yan, and W.-C. Jiang, Roles of the transition amplitude phases in photoelectron asymmetry of single strong attosecond pulse, New J. Phys. **24**, 093019 (2022).

[35] K. B. Whaley and J. C. Light, Rotating-frame transformations: A new approximation for multiphoton absorption and dissociation in laser fields, Phys. Rev. A **29**, 1188 (1984).

[36] W. P. Schleich, *Quantum Optics in Phase Space* (John Wiley & Sons, New York, 2011).

[37] J. M. Ngoko Djiokap, S. X. Hu, L. B. Madsen, N. L. Manakov, A. V. Meremianin, and A. F. Starace, Electron Vortices in Photoionization by Circularly Polarized Attosecond Pulses, Phys. Rev. Lett. **115**, 113004 (2015).

[38] J. M. Ngoko Djiokap, A. V. Meremianin, N. L. Manakov, S. X. Hu, L. B. Madsen, and A. F. Starace, Multistart spiral electron vortices in ionization by circularly polarized UV pulses, Phys. Rev. A **94**, 013408 (2016).

[39] M. Anand, S. Pabst, O. Kwon, and D. E. Kim, Attosecond counter-rotating-wave effect in xenon driven by strong fields, Phys. Rev. A **95**, 053420 (2017).

[40] W.-C. Jiang and X.-Q. Tian, Efficient split-lanczos propagator for strong-field ionization of atoms, Opt. Express **25**, 26832 (2017).

[41] W.-C. Jiang, S.-G. Chen, L.-Y. Peng, and J. Burgdörfer, Two-Electron Interference in Strong-Field Ionization of He by a Short Intense Extreme Ultraviolet Laser Pulse, Phys. Rev. Lett. **124**, 043203 (2020).

[42] S. Wang, W.-C. Jiang, X.-Q. Tian, and H.-B. Sun, Conjoint influence of quantum interference and Freeman resonance on substructures of the photoelectron spectra in above-threshold ionization, Phys. Rev. A **101**, 053417 (2020).

[43] T. N. Rescigno and C. W. McCurdy, Numerical grid methods for quantum-mechanical scattering problems, Phys. Rev. A **62**, 032706 (2000).

[44] B. I. Schneider and L. A. Collins, The discrete variable method for the solution of the time-dependent Schrödinger equation, J. Non-Cryst. Solids **351**, 1551 (2005).

[45] M. J. Rayson, Lagrange-Lobatto interpolating polynomials in the discrete variable representation, Phys. Rev. E **76**, 026704 (2007).

[46] L. Geng, H. Liang, and L.-Y. Peng, Laser-induced electron fresnel diffraction in tunneling and over-barrier ionization, Chin. Phys. Lett. **39**, 044203 (2022).

[47] X. M. Tong, K. Hino, and N. Toshima, Phase-dependent atomic ionization in few-cycle intense laser fields, Phys. Rev. A **74**, 031405(R) (2006).

[48] U. Fano, Propensity rules: An analytical approach, Phys. Rev. A **32**, 617 (1985).

[49] D. Busto, J. Vinbladh, S. Zhong, M. Isinger, S. Nandi, S. Maclot, P. Johnsson, M. Gisselbrecht, A. L'Huillier, E. Lindroth, and J. M. Dahlström, Fano's Propensity Rule in Angle-Resolved Attosecond Pump-Probe Photoionization, Phys. Rev. Lett. **123**, 133201 (2019).

[50] E. Foumouo, A. Hamido, P. Antoine, B. Piraux, H. Bachau, and R. Shakeshaft, Time-dependent analysis of the mechanism for two-photon double escape in helium: from very long to attosecond time scales, J. Phys. B **43**, 091001 (2010).

[51] J. M. Ngoko Djiokap, N. L. Manakov, A. V. Meremianin, S. X. Hu, L. B. Madsen, and A. F. Starace, Nonlinear Dichroism in Back-to-Back Double Ionization of He by an Intense Elliptically Polarized Few-Cycle Extreme Ultraviolet Pulse, Phys. Rev. Lett. **113**, 223002 (2014).

[52] L.-Y. Peng, E. A. Pronin, and A. F. Starace, Attosecond pulse carrier-envelope phase effects on ionized electron momentum and energy distributions: Roles of frequency, intensity and an additional IR pulse, New J. Phys. **10**, 025030 (2008).

[53] A. Messiah, *Quantum Mechanics-Two Volumes Bound as One*, 1st ed. (Dover, Mineola, NY, 1999).

[54] W.-C. Jiang and J. Burgdörfer, Dynamic interference as signature of atomic stabilization, Opt. Express **26**, 19921 (2018).

[55] W.-C. Jiang, M.-X. Wang, L.-Y. Peng, and J. Burgdörfer, Signatures of stabilization in the angle-resolved photoemission by an ultrashort intense XUV laser pulse, Phys. Rev. A **105**, 023104 (2022).

[56] J. Su, H. Ni, A. Jaroń-Becker, and A. Becker, Time Delays in Two-Photon Ionization, Phys. Rev. Lett. **113**, 263002 (2014).